

Improving the Fractional Order PID Controller Performance with an Energy Storage System for Photovoltaics

TAREK A. BOGHDADY, ALI J. ALAMER, M. A. MOUSTAFA HASSAN, A. A. SEIF
Department of Electrical Engineering, Faculty of Engineering
Cairo University
Giza, Egypt
EGYPT

Abstract: - A PhotoVoltaic (PV) dependent maximum power point tracking controller is used, modeled, and assessed. It includes a study of system components and their modelling. The model is then tested and validated using more than one method. This article focuses on increasing energy extraction in grid-connected PV and isolated systems, damping system oscillations, and reducing its settling time. Tuning the PID controller and the fractional order PID controller is a challenging task that can be carried out by trial and error, Ziegler-Nichols method, or by optimization techniques. In this article; genetic algorithms and whale optimization algorithms are being used here to obtain desired controller response by minimizing the objective function. The objective function is the integral square error. A PV is proposed to use a Fractional Order PID (FOPID) controller then compared to its conventional PID controller. The results show that the output power has a faster response and eliminates oscillations around the maximum power point under steady-state conditions. The results confirm that the proposed controller with an energy storage system has improved energy extraction. All simulations were carried out using MATLAB/SIMULINK.

Key-Words: - Genetic Algorithm, FOPID, Photovoltaics, Renewable Energy, Whale Optimization Algorithm.

Received: April 12, 2021. Revised: January 23, 2022. Accepted: February 12, 2022. Published: March 3, 2022.

1 Introduction

As the world faces a challenge to overcome the energy crisis. The decreasing deposits of non-renewable energy resources such as coal, natural gas, fossil fuels, etc. have raised awareness of such crisis. So, it has become a necessity to develop new ways to replace traditional energy sources. Solar energy is a renewable, inexhaustible, and ultimate source of energy. If used properly, it can fulfil numerous energy needs of the world. The power from the sun intercepted by the earth is approximately 1.8×10^{11} MW [1-5]. This amount of energy is thousands of times larger than the current consumption rate. Thus clarifies the importance of renewable energy in general and solar energy in particular. Solar energy is the source of all energies on Earth. Fossil fuel is a storage of this energy over a large period. Also, the wind is moved by temperature difference caused by solar irradiance.

The PhotoVoltaic (PV) system consists of interconnected components designed to achieve the specific target of delivering desired electricity from a small device to the load. PV systems are categorized by the main categories of grid-connected, stand-alone systems and hybrid systems, which comprise of different energy sources such as

PV arrays, diesel generators, and wind generators. In grid-connected and stand-alone systems, storage elements such as batteries, fuel cells, or supercapacitors may be adapted to store energy during daytime. The systems are modelled using an energy storage element such as a battery storage, supercapacitor, and then both; then without energy storage. While the PV panels may seem like a good source of electricity, their conversion efficiency is not very high; with high cost and low efficiency (from 9-17%) [6]. Therefore, if the load is coupled directly to the PV array, the PV array must usually be oversized to supply required load power. This leads to an oversized expensive system. Thus, PV arrays should be operated at the Maximum Power Point (MPP) which changes with different solar irradiances and load variations. Several Maximum PowerPoint Tracking (MPPT) techniques have been developed for PV systems [7]. The main problem is how to obtain optimal operating points (voltage & current) automatically at maximum PV output power under variable atmospheric conditions.

This paper is organized as follows: System modeling including PV and DC-DC converter a battery is introduced in Section 2 to select one of them for the PI and FOPI tuning problem a

comparison is carried out in Section 3 results and discussion are stated. Finally, Section 4 summarizes the simulation results.

2 System Modelling

2.1 PV Modelling

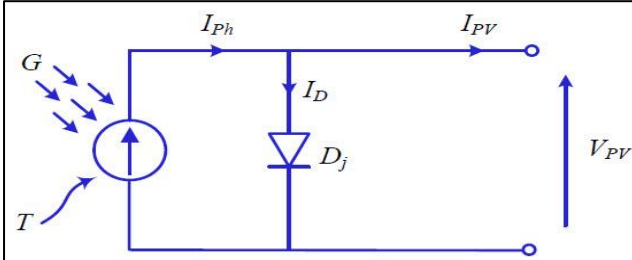


Fig. 1: A simple ideal equivalent circuit of a PV cell.

From Figure 1 and by applying Kirchhoff's current law,

$$I_{PV} = I_{ph} - I_D \quad (1)$$

Where I_D is the diode internal diffusion current, I_{ph} is the photocurrent or light generated current, which is proportional to the radiation and surface temperature. The output current and voltage of the solar cell are represented by I_{PV} and V_{PV} , respectively. The diode internal diffusion current is modelled by Equation (2) [8].

$$I_D = I_s \left[e^{\left(\frac{q \cdot V_{PV}}{A \cdot K \cdot T_c} \right)} - 1 \right] \quad (2)$$

Where q is the electron charge, 1.6×10^{-19} C, A is the diode ideality factor and takes the value between 1 and 2, K is Boltzmann's constant, 1.38×10^{-23} J/K. T_c is the cell's operating temperature in kelvin and I_s is the cell saturation current, which varies with temperature according to Equation (4), as stated in [4]. Equation (3) calculates I_{ph} the photocurrent related to the cell's operating temperature and solar intensity.

$$I_{ph} = \left[I_{sc} + K_t \cdot (T_c - T_{Ref}) \right] \cdot \frac{G}{G_{Ref}} \quad (3)$$

Where I_{sc} is the short-circuit current known from the datasheet, K_t is the cell's short circuit temperature coefficient (Amperes/ K), T_{Ref} is the cell reference temperature in kelvin, $T_{Ref} = 298$ K (25°C), G is the solar irradiance in W/m^2 , and G_{Ref} represents the reference solar irradiance W/m^2 , $G_{Ref} = 1 \text{ kW}/\text{m}^2$ [4]. The short circuit current is measured

under the standard test condition at a reference temperature of 25°C and solar irradiance $1 \text{ kW}/\text{m}^2$.

$$I_{sc} = I_{RS} \cdot \left(\frac{T_c}{T_{Ref}} \right)^3 \cdot e^{\left(\frac{q \cdot E_g}{A \cdot K} \cdot \left(\frac{1}{T_{Ref}} - \frac{1}{T_c} \right) \right)} \quad (4)$$

In Equation (4), I_{RS} is the cell's reverse saturation current in Ampere at T_{Ref} , and the solar irradiance $1 \text{ kW}/\text{m}^2$. E_g is the band-gap energy of the cell's semiconductor used. The cell's reverse saturation current at reference temperature can be obtained by Equation (5) [8].

$$I_{RS} = \frac{I_{sc}}{e^{\left(\frac{q \cdot V_{OC}}{A \cdot K \cdot T_{Ref}} \right)} - 1} \quad (5)$$

Where V_{OC} is the open-circuit voltage at reference temperature T_{Ref} .

To account for the losses that occur inside a solar cell, R_s (series resistance) and R_{sh} (parallel resistance) are to be included in this model as shown in Figure 2.

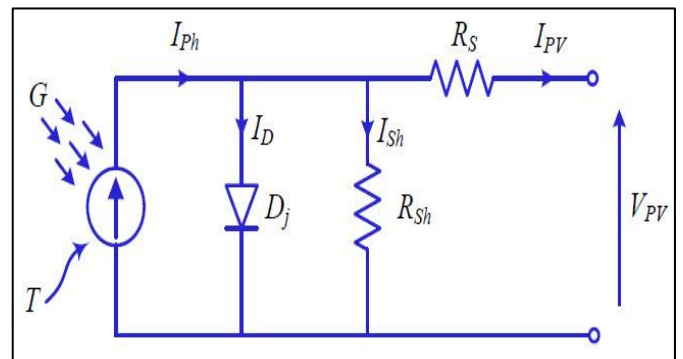


Fig. 2: An exact equivalent circuit for a PV cell.

Hence the PV cell output current I_{PV} , in Figure 2 is given by Equation (6) [8].

$$I_{PV} = I_{ph} - I_s \cdot \left[e^{\left(\frac{q \cdot (V_{PV} + I_{PV} \cdot R_s)}{A \cdot K \cdot T_c} \right)} - 1 \right] - \frac{V_{PV} + I_{PV} \cdot R_s}{R_{sh}} \quad (6)$$

The shunt resistance, R_{sh} , represents the shunt leakage current to the ground due to p-n junction non-ideal ties and impurities near the junction. The series resistance R_s is due to semiconductor-material bulk resistance, the metal contact particularly that of the front grid, and the transverse flow of current in the solar emitter to the front grid.

In general, the variation of R_{sh} does not affect the PV cell short circuit current, I_{sc} , but it reduces the PV cell open-circuit voltage. Without leakage current to the ground, R_{sh} can be assumed to be

infinite. On the other hand, a small variation in R_S leads to a reduction in the short-circuit current but does not affect the open-circuit voltage therefore the maximum power changes significantly according to [9].

As mentioned above, the small variation in R_S has a significant effect on the PV panel output power. On the other hand, the PV efficiency is insensitive to variation in R_{Sh} , which can be assumed to approach infinity without leakage current. Therefore, R_{Sh} can be neglected to give appropriate model with suitable complexity.

By neglecting the shunt resistance, as shown in Figure 3, Equation (7) can be written as [4]:

$$I_{PV} = I_{ph} - I_S \cdot \left[e^{\left(\frac{q \cdot (V_{PV} + I_{PV} \cdot R_S)}{A \cdot K \cdot T_c} \right)} - 1 \right] \quad (7)$$

According to reference [10], the value of R_S can also be calculated by Equation (8).

$$R_S = \frac{V_{OC} - V_{PV} + \frac{A \cdot K \cdot T_c}{q} \cdot \ln\left(1 - \frac{I}{I_{sc}}\right)}{I_{sc}} \quad (8)$$

By using the method of panel modelling that was introduced in [11] with the related equivalent circuit as shown in Figure 2, a PV panel must be selected first. For this work, PWX 500 (49 Watt-peak) panel is chosen. The specifications of the PV panel from its datasheet including the electrical ones are shown in Table A.1.

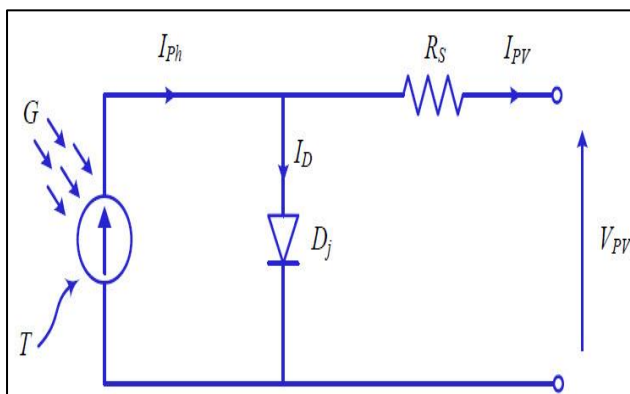


Fig. 3: An appropriate equivalent circuit model.

The next step is to implement Equations (1) through (8) as a MATLAB/SIMULINK model using previously specified parameters. Its inputs are solar irradiance (G) and cell temperature (T), and its outputs are the related panel voltage and current.

By looking under this mask, the PV current source is modelled by a controlled current source whose value is calculated from equations depending on the

current solar irradiance (G). The inputs for this subsystem are solar irradiance and temperatures. The outputs are the PV panel output current and voltage as Simulink signals and two physical modelling ports to connect the panel with the DC-DC converter.

2.2 DC-DC Converter Modelling

According to [12] the worst case is found at lowest resistance for DC-DC boost converters to stay at the continuous current mode (CCM). Hence, The MPP capture will only be possible for load resistance (R_L) values higher than or equal to the resistance at maximum power point (RMPP), the minimum used load resistance in the simulations equals 10Ω . Table 1 shows the specification values, from the datasheet values for the PV module in Table A.1, used to design the DC-DC boost converter parameters.

The converter duty ratio, D , can be calculated from Equation (9) as discussed in [14]

$$D = 1 - \frac{V_d}{V_o} \quad (9)$$

Where D denotes the duty ratio. V_d and V_o denote the input and output voltages of the boost converter, respectively. From the previous equation, the increase in duty ratio D will increase the value of the output voltage, V_o .

Additionally; the change in duty ratio results in an input and output converter current change. The filter inductor and capacitor to operate the converter in the continuous conduction mode can be calculated by the following equations [14]:

$$L = \frac{V_d \cdot D}{2 \cdot \Delta I_L \cdot f_s} \quad (10)$$

$$C = \frac{I_o \cdot D}{\Delta V_o \cdot f_s} \quad (11)$$

Where I_o is the output current, f_s is the switching frequency, Δ denotes the variation, L is the inductor value and C is the capacitor value.

Table 1. Specification values for the design of DC-DC boost converter parameters.

Specification	Value
Input voltage	17 V
Input current	2.88 A.
Output voltage (V_o)	21.5 V
Voltage ripples (ΔV_o)	5 %
Current ripples (ΔI_L)	5 %
Output power of the PV @ 1000 w/m ²	49 W.
Switching Frequency (f_s)	10 kHz

Hence, we can calculate the values of I_L , ΔV_o , ΔI_L as follows:

$$P_o = I_L * V_o$$

Assuming 100% converter efficiency: $P_o = P_{in}$

$$\therefore I_L = \frac{P_o}{V_o} = \frac{49}{21.5} = 2.279 \text{ Amp}$$

$$\Delta I_L = 0.05 * I_L = 0.05 * 2.279 = 0.11395 \text{ Amp}$$

$$\Delta V = 0.05 * V_o = 0.05 * 21.5 = 1.075 \text{ Volt}$$

Using Equation 11: $D = 1 - \frac{17}{21.5} = 0.2093$

Using Equation 12: $L = \frac{17 * 0.2093}{2 * 10^4 * 0.11395} = 1.56 \text{ mH}$

Using Equation 13: $C = \frac{2.279 * 0.2093}{10^4 * 1.075} = 443.73 \mu\text{F}$

2.3 Battery Sizing

For models with batteries, a constant power load is used. The load is 40 Watts at 12 V. For this load, the battery sizing is done as follows [13]:

Total AH needed = $160 / 0.8 = 200 \text{ AH}$

3 PID and Fractional Order PID (FOPID) Controller Testing

To test the system, three solar irradiance schemes are used. The first is a uniform step change, where radiation starts at maximum radiation (1000 W/m^2) and drops to 600 W/m^2 at 0.3 sec., then increases to 800 W/m^2 at 0.9 sec., and fixed. This is shown in Figure 4. The second is the droop and raise scheme where the radiation starts at 0 sec. with a value of 600 W/m^2 and decreases linearly to 400 W/m^2 at 0.4 sec. Then it increases to 700 W/m^2 and increases linearly to 1000 W/m^2 at 0.6 sec. Then it drops to 600 W/m^2 and increases linearly to 800 W/m^2 at 1 sec. This is shown in Figure 5. The third and last is that based on the medium-high ramp change according to British standards (B.S.) EN50530 [14]. This is shown in Figure 6. The optimization algorithms will be tested first.

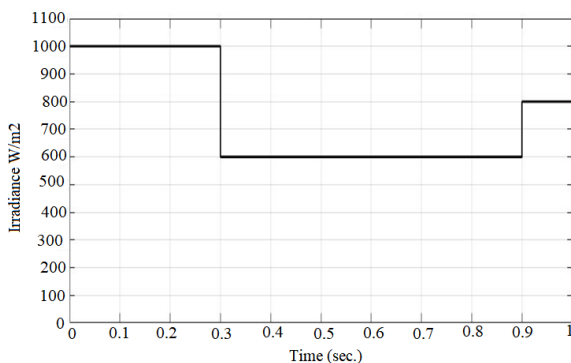


Fig. 4: Uniforms step-change Radiation Scheme.

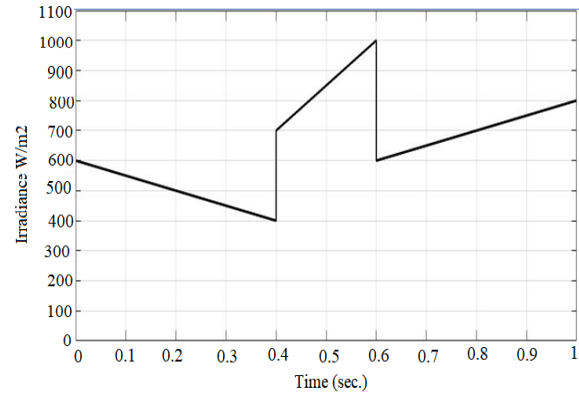


Fig. 5: Droop/Raise Radiation Scheme.

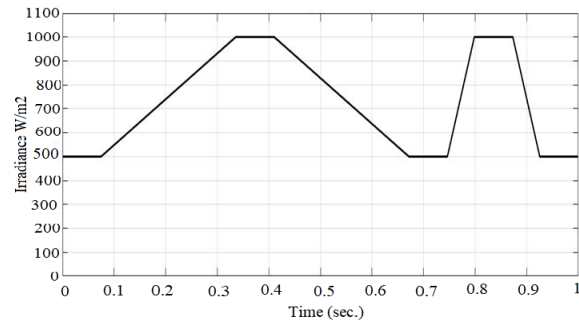


Fig. 6: B.S. EN50530 Radiation Change.

3.1 Testing/Comparing Whale Optimization Algorithm (WOA) with Other Algorithms

Improving controller performance by tracing the reference signal “(i.e. reducing the error between measured and reference signals)” of an industrial process is an important task by using traditional PID controller, but finding optimum value of PID control parameters is a very difficult issue. Most PID tuning techniques use conventional methods such as frequency response which requires considerable technical experience to apply those formulas. Due to their difficulties, PID controller parameters are rarely tuned optimally.

The aim here is to test WOA [15] and carry out a comparison between its performance with PSO, GA, and Linearized Biogeography-Based Optimization (LBBO) [16-19]. The squared error integral criteria are the objective function to be minimized in the step response of a process which is cascaded with a PID controller as shown in Figure 7 by tuning proportional gain (K_p), integral gain (K_i), and differential gain (K_d) using MATLAB/SIMULINK.

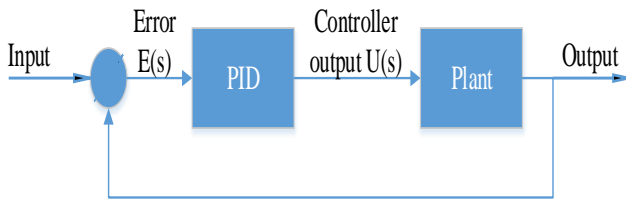


Fig. 7: Block Diagram of Tested Systems

Table 2 shows seven transfer functions of benchmark systems of different orders that will be used here for testing WOA performance. The tuned gains obtained by using WOA algorithm are given in Table 2, while Table 3 presents tuned gains that have been obtained using three algorithms.

For the first plant, values of Kp, Ki, and Kd founded by WOA, GA, and LBBO are nearly the same, while Particle Swarm Optimization (PSO) solution is drifted by about 40% of the values found by other algorithms. This is reflected in the objective function values as shown in Table 4 where PSO has the worst objective function value. The results of three algorithms (WOA, GA, and LBBO) applied to plants 2, 4, and 6 are nearly the same optimized value. For plant 4 the PSO algorithm result has an unstable solution, while solutions found by the three other algorithms are almost the same. Also, it is obvious that results obtained by WOA in plants 3, 5, and 7 is much better than all other algorithms, the WOA has approximately a reduction from 21% to 45% in the optimized value.

Table 4 (the lowest value in each row is shown in black boldface) indicates that WOA produces better results with a lower number of the objective function evaluation. The unit step response for the test plants using the four optimization algorithms PSO, GA, LBBO, and WOA for tuning the PID parameters are shown in Figure 8 through Figure 14. In all cases, WOA has the fastest settling time.

Table 2. Tuned Values Obtained by WOA

Plant No.	Transfer Function	WOA		
		Kp	Ki	Kd
1	$\frac{5}{S^4 + 3S^3 + 7S^2 + 5S}$	1.416	0	1.124
2	$\frac{S + 5}{S^4 + 17S^3 + 60S^2 + 10S}$	30	0	19.02

3	$\frac{300(S + 100)}{S(S + 10)(S + 40)}$	25	0	0.416
4	$\frac{6}{S^4 + 3S^3 + 4S^2 + 3S + 1}$	0.325	0.097	0.488
5	$\frac{250S + 500}{S^3 + 12S^2 + 100S + 10}$	9.7.32	6.928	0.175
6	$\frac{S + 5}{S^4 + 17S^3 + 60S^2 + 5S}$	15	0.942	13.78
7	$\frac{1}{S^2 + 0.1S + 1}$	10	2.523	2.923

Table 3. Tuned Values for LBBO, GA, PSO.

Plant No.	LBBO			GA			PSO		
	Kp	Ki	Kd	Kp	Ki	Kd	Kp	Ki	Kd
1	1.4	0.0	1.0	1.0	0	1.0	0.6	0	0.6
2	29	0	19	25	0	12	4.4	0	14
3	24	1	1.0	25	0.3	10	0.2	0	0.0
4	0.3	0.1	0.4	0.2	0.1	0.4	0.1	0.5	16
5	4.2	3.3	0.1	1	1	0	0.4	0.2	0.2
6	15	0.8	13	14	1	13	3.7	0.1	13
7	6.1	1.1	5.0	4.0	1	3.0	0.7	1.1	3.6

Table 4. Objective Function Values Obtained by WOA, LBBO, Genetic Algorithm, and PSO.

Plant No.	Best Min. Objective Function			
	WOA	LBBO	GA	PSO
1	1.1102	1.3132	1.9746	1.9520
2	0.6007	0.6497	0.6505	2.2400
3	0.0099	0.0105	0.216	0.1469
4	1.9101	1.9392	2.1500	21.7600
5	0.0206	0.0239	0.3661	0.3697
6	0.8737	0.9078	0.9513	2.5600
7	0.2153	0.2952	0.5374	1.5330

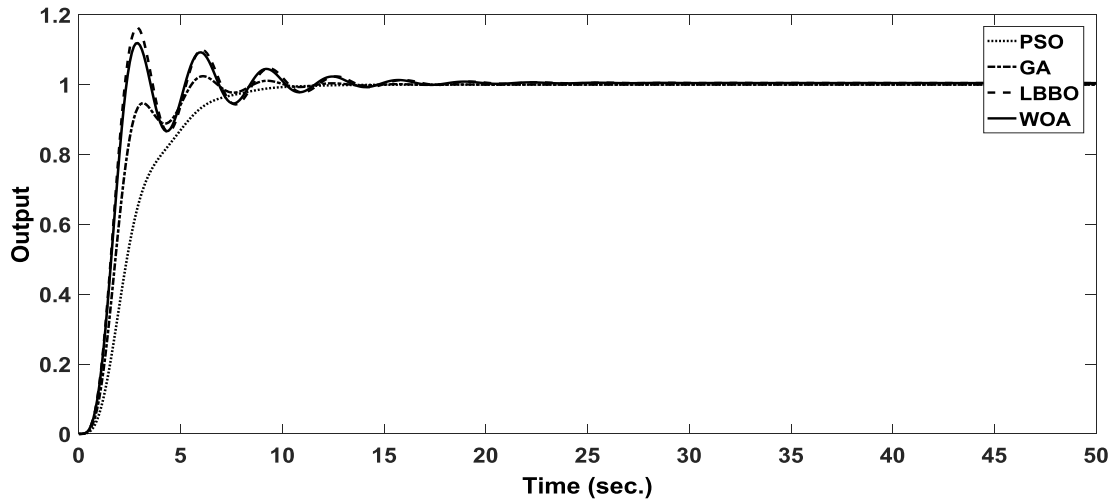


Fig. 8: Plant 1 - Output Response.

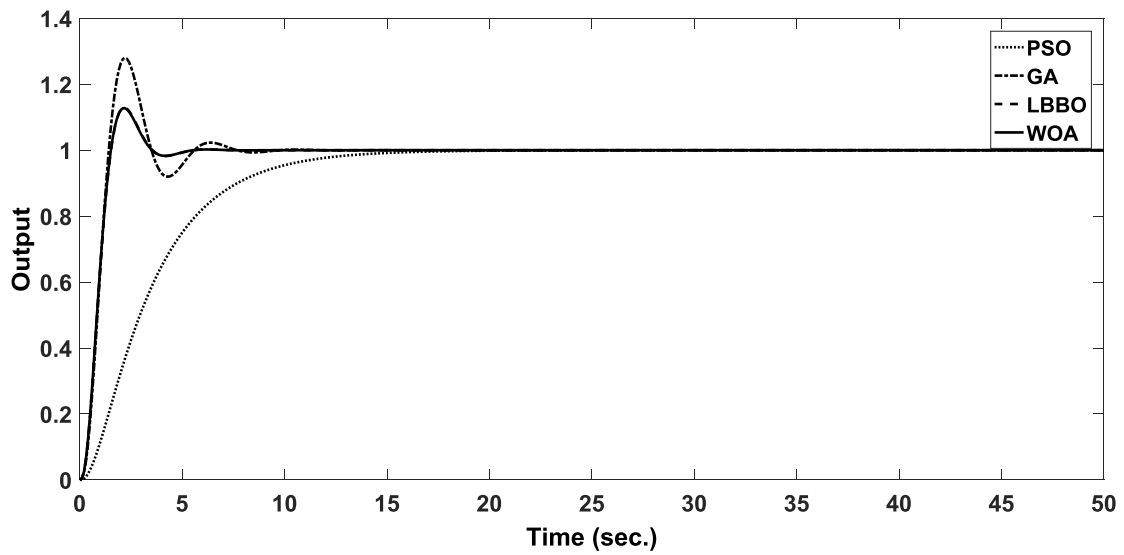


Fig. 9: Plant 2 - Output Response.

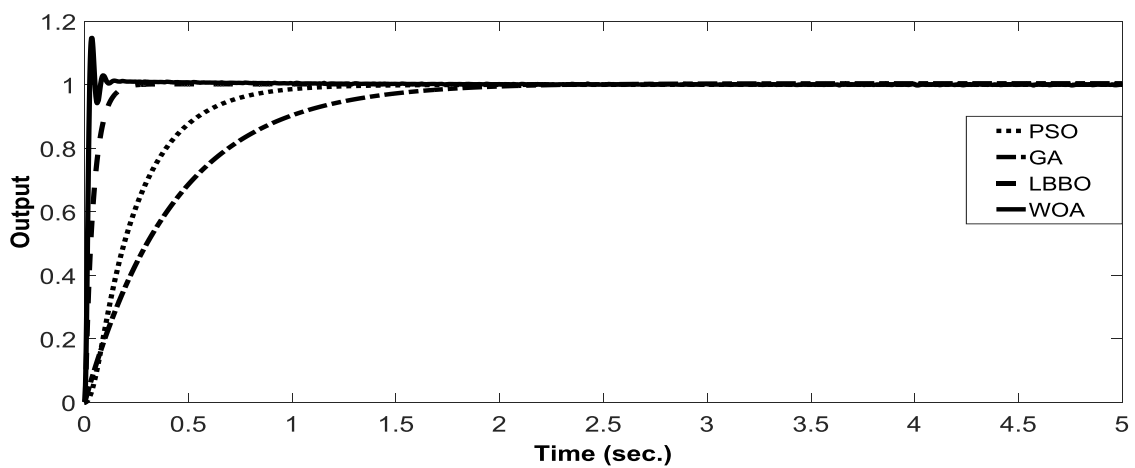


Fig. 10: Plant 3 - Output Response.

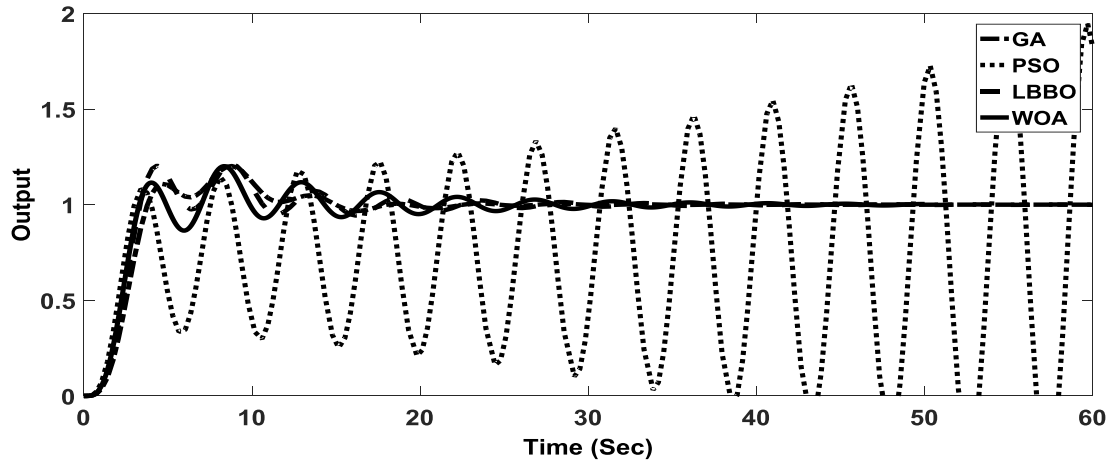


Fig. 11: Plant 4 – Output Response

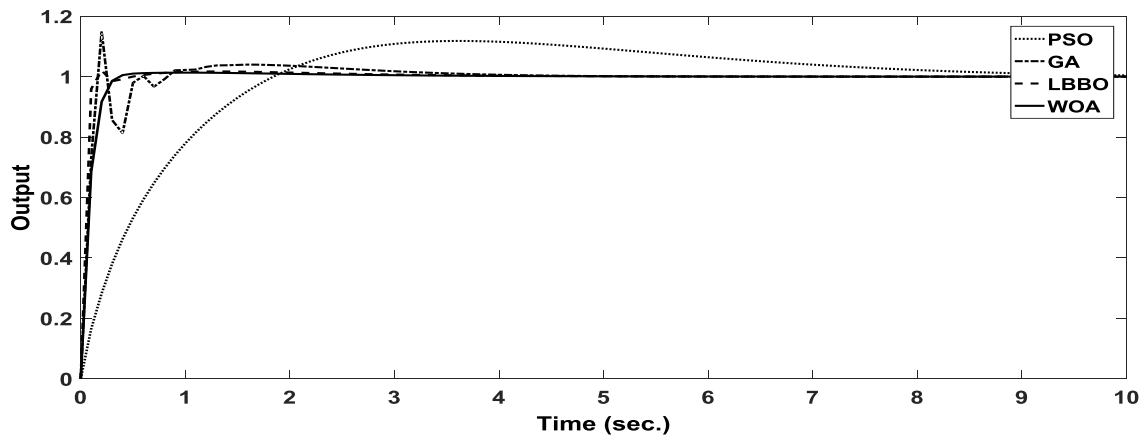


Fig. 12: Plant 5 - Output Response.

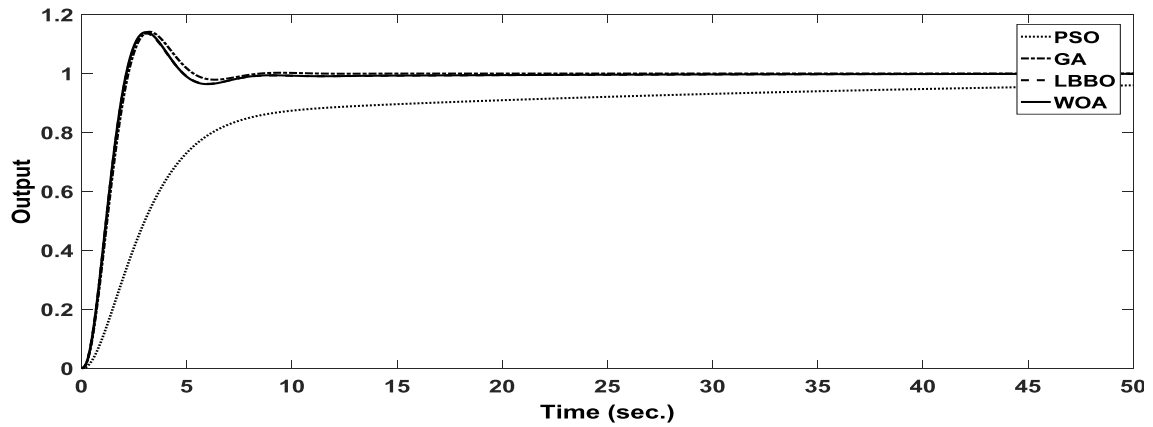


Fig. 13: Plant 6 - Output Response.

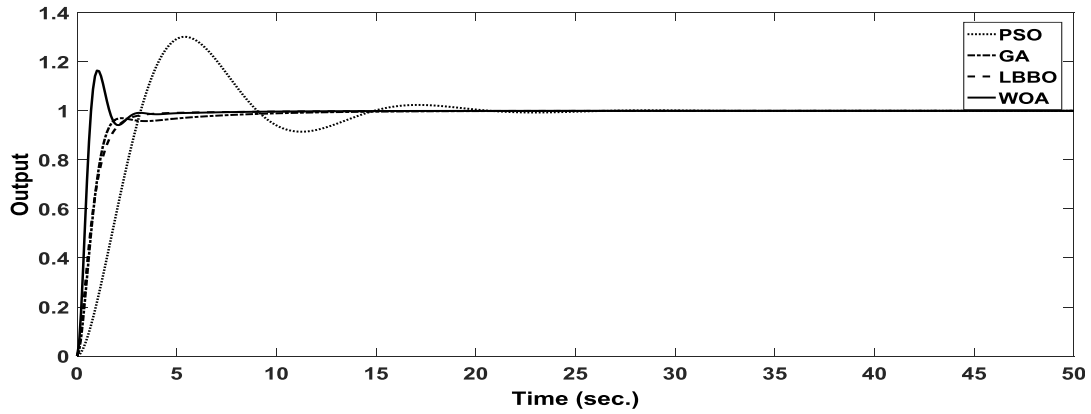


Fig. 14: Plant 7 - Output Response

In the next section, the obtained power curve using PI and FOPI tuned by WOA. The input solar irradiances are stated before, uniform step change, droop/raise, and EN50530 radiations, shown in Figures 4 to 6, those curves will test the controller performance. The outputs are shown in Figures 15 to 20. FOPI has a faster response than PI (i.e. lower rising and settling time) with lower oscillations. Also, captured obtained energy by FOPI is higher in the three tested radiations. It is also noticed that the cell reached its rated power (49 W) in all cases for FOPI controller while PI approximately reached it only in uniform step-change radiation. FOPI has a lower overshoot in all cases.

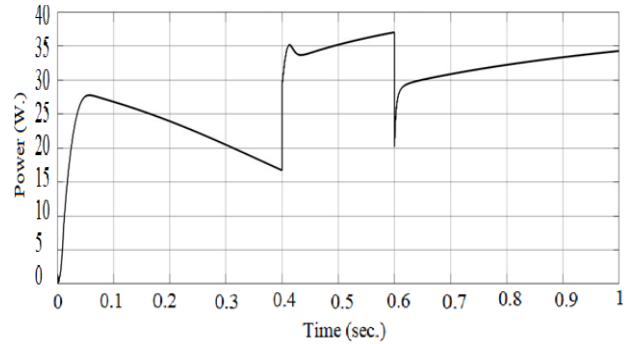


Fig. 17: PV Output Power Droop/Raise Solar Irradiance using PI.

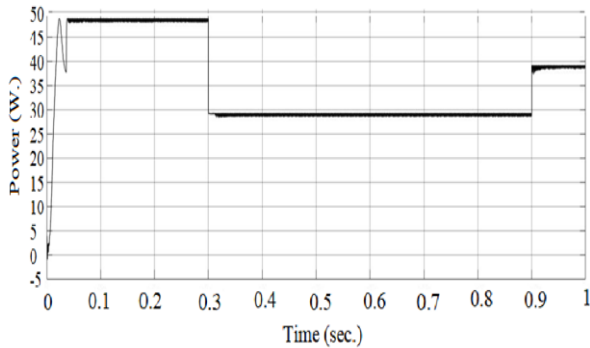


Fig. 15: PV Output Power Uniform Step-Change Solar Irradiance using PI.

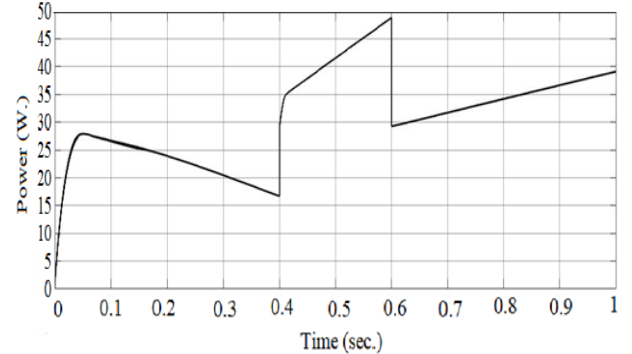


Fig. 18: PV Output Power Droop/Raise Solar Irradiance using FOPI.

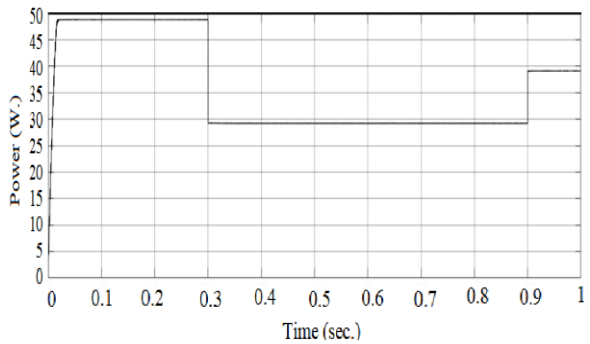


Fig. 16: PV Output Power Uniform Step-Change Solar Irradiance using FOPI.

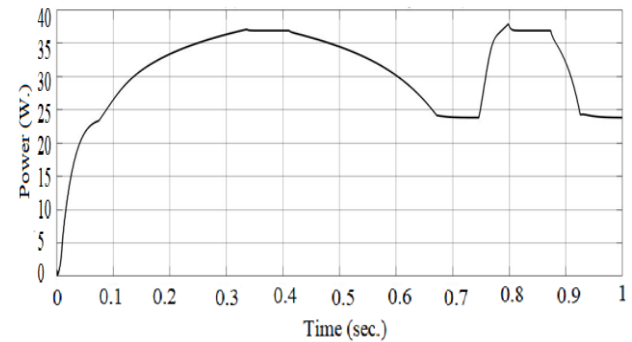


Fig. 19: PV Output Power with EN50530 Solar Irradiance using PI.

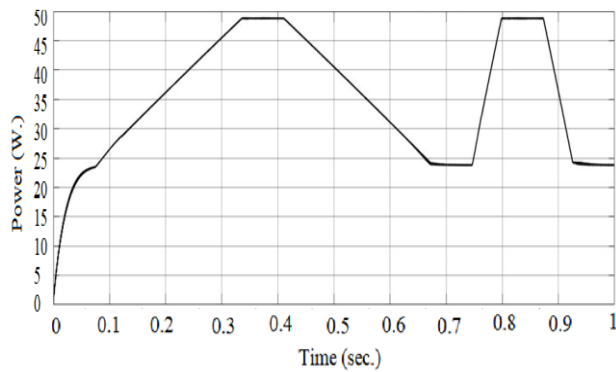


Fig. 20: PV Output Power with EN50530 Solar Irradiance using FOPI.

4 Conclusions

Each PV system part discussed in this article, is modelled using MATLAB/SIMULINK software such as PV and DC-DC converter and the battery. Further, a comparison between optimization algorithms is carried out; showing that WOA was the best tool for FOPI tuning problem. All output Tables and Figures assured that FOPI has better performance; lower variations and faster settling also in capturing MPP.

Appendix A

Table A.1 Specifications of Simulated PV Module, PWX-500 [20]

Parameter	Value
P_{max} (W)	49
I_{MPP} (A)	2.88
V_{MPP} (V)	17
I_{sc} (A)	3.11
V_{oc} (V)	21.8
R_s (Ω)	0.55
R_p (Ω)	50000
Normal Operating Cell Temperature (NOCT) (C°)	45

References

- [1] Messenger, Roger A., and Amir Abtahi. Photovoltaic systems engineering. CRC press, 2018.
- [2] T. A. Boghdady, Ali J. Alamer, Mina M. Yousef, Ahmed M. Elshafee, M. A. Mostafa Hassan, A. Monem Seif, "Technical and Economic Study of Powering Poultry Farm in Egypt using PV-Biomass on-grid Energy Generation System: Case Study", WSEAS Transactions on Power Systems, vol. 16, pp. 67-77, 2021.
- [3] Ammaiyappan, A. Bharathi Sankar, and R. Seyezhai. "Implementation of Fuzzy logic control based MPPT for Photovoltaic system with Silicon Carbide (SiC) boost DC-DC converter." WSEAS Transactions on Systems and Control 16 (2021): 198-215.
- [4] Ahmed, Razin, et al. "A review and evaluation of the state-of-the-art in PV solar power forecasting: Techniques and optimization." Renewable and Sustainable Energy Reviews 124 (2020): 109792.
- [5] Türk, Seda, Ahmet Koç, and Gökhan Şahin. "Multi-criteria of PV solar site selection problem using GIS-intuitionistic fuzzy based approach in Erzurum province/Turkey." Scientific Reports 11.1 (2021): 1-23.
- [6] Kinal Kachhiya, Makarand Lokhande, Mukesh Patel, 2011, "MATLAB/SIMULINK model of solar PV module and MPPT algorithm", National conference on recent trends in engineering & technology, May 2011.
- [7] Yang, Bo, et al. "Comprehensive overview of maximum power point tracking algorithms of PV systems under partial shading condition." Journal of Cleaner Production 268 (2020): 121983.
- [8] Fathi A. O. Aashoor, May 2015, "Maximum Power Point Tracking Techniques for Photovoltaic Water Pumping System", University of Bath.
- [9] Luís R. A. Gabriel Filho, Daniel Dos S. Viais Neto, Camila P. Cremasco, Odivaldo J. Seraphim, Fernando De L. Caneppele, 2012, "Mathematical Analysis Of Maximum Power Generated By Photovoltaic Systems And Fitting Curves For Standard Test Conditions", Eng. Agric., Jaboticabal, Vol.32, No.4, July 2012, p.650-662.
- [10] Zhang, Guidong, et al. "Power electronics converters: Past, present and future." Renewable and Sustainable Energy Reviews 81 (2018): 2028-2044.
- [11] Mohamed, M. A., Ahmed Elnozahy, and ALMOATAZ Y. Abdelaziz. "Optimal energy saving of photovoltaic distributed generation system with considering environment condition via hyper-spherical search algorithm." WSEAS Transactions on Power Systems 13 (2018): 311-325.
- [12] Nicola Femia, Giovanni Petrone, Giovanni Spagnuolo and Massimo Vitelli, 2013, "Power Electronics and Control Techniques for Maximum Energy Harvesting in Photovoltaic Systems", CRC Press.

- [13] Manoharan, Premkumar, et al. "Improved perturb and observation maximum power point tracking technique for solar photovoltaic power generation systems." *IEEE Systems Journal* 15.2 (2020): 3024-3035.
- [14] Coppitters, Diederik, Ward De Paepe, and Francesco Contino. "Surrogate-assisted robust design optimization and global sensitivity analysis of a directly coupled photovoltaic-electrolyzer system under techno-economic uncertainty." *Applied Energy* 248 (2019): 310-320.
- [15] Zenhom, Z. M., and T. A. Boghdady. "Optimal Allocation of Distributed Generation in A Part of The Egyptian Electrical Network Using Whale Optimization Algorithm." 2019 21st International Middle East Power Systems Conference (MEPCON). IEEE, 2019.
- [16] Tarek A. Boghdady, MM sayed, and Essam A Elzahab. "Maximization of Wind Energy Conversion Using Sliding Mode Control Tuned By Linearized Biogeography-Based Optimization." *Journal of Electrical Engineering* 15.4 (2015): 69-74.
- [17] Tarek A. Boghdady, MM sayed, and Essam A Elzahab. "An Analysis of Migration Models for Linearized Biogeography-Based Optimization Applied for PID Tuning Problem." *Journal of Electrical Engineering* 16.1 (2016): 257-268.
- [18] Boghdady, T. A., and M. M. Sayed. "Improving the performance of HVDC system using Fuzzy PI controller tuned by Linearized Biogeography-Based Optimization Algorithm." (2018): 12-5.
- [19] Boghdady, T. A., Sayed, M. M., Emam, A. M., & El-Zahab, E. A. (2014, December). A novel technique for PID tuning by linearized biogeography-based optimization. In 2014 IEEE 17th International Conference on Computational Science and Engineering (pp. 741-747). IEEE.
- [20] Ali M. Humada, Mojgan Hojabri, Saad Mekhilef, Hussein M. Hamada, 2016," Solar cell parameters extraction based on single and double-diode models: A review", *Renewable and sustainable energy reviews*, Vol.56, April 2016, Pages 494–509.

**Creative Commons Attribution License 4.0
(Attribution 4.0 International, CC BY 4.0)**

This article is published under the terms of the Creative Commons Attribution License 4.0

https://creativecommons.org/licenses/by/4.0/deed.en_US